Range Extension of Light-Duty Electric Vehicle Improving Efficiency and Power Density of IPMSM Considering Driving Cycle

주행 사이클을 고려한 IPMSM의 효율 및 출력 밀도 개선으로 경량 전기 자동차의 주행거리 연장

저자 (Authors) Dong-Min Kim, Young-Hoon Jung, Myung-Seop Lim, Jae-Han Sim, Jung-Pyo Hong

출처 (Source) 전기학회논문지 65(12), 2016.12, 2197-2210(14 pages)
The transactions of The Korean Institute of Electrical Engineers 65(12), 2016.12, 2197-2210(14 pages)

발행처 (Publisher) 대한전기학회
The Korean Institute of Electrical Engineers

URL http://www.dbpia.co.kr/journal/articleDetail?nodeId=NODE07067058

APA Style Dong-Min Kim, Young-Hoon Jung, Myung-Seop Lim, Jae-Han Sim, Jung-Pyo Hong (2016). Range Extension of Light-Duty Electric Vehicle Improving Efficiency and Power Density of IPMSM Considering Driving Cycle. 전기학회논문지, 65(12), 2197-2210

ISSN 1975-8359(Print) / ISSN 2287-4364(Online)
The Transactions of the Korean Institute of Electrical Engineers Vol. 65, No. 12, pp. 2197~2210, 2016
http://dx.doi.org/10.5370/KIEE.2016.65.12.2197

주행 사이클을 고려한 IPMSM의 효율 및 출력 밀도 개선으로 경량 전기 자동차의 주행거리 연장

Range Extension of Light-Duty Electric Vehicle Improving Efficiency and Power Density of IPMSM Considering Driving Cycle

김 동 민* · 정 영 훈* · 임 명 섭* · 심 재 한* · 홍 정 표†
(Dong-Min Kim · Young-Hoon Jung · Myung-Seop Lim · Jae-Han Sim · Jung-Pyo Hong)

Abstract - Recently, the trend of zero emissions has increased in automotive engineering because of environmental problems and regulations. Therefore, the development of battery electric vehicles (EVs), hybrid/plug-in hybrid electric vehicles (HEVs/PHEVs), and fuel cell electric vehicles (FCEVs) has been mainstreamed. In particular, for light-duty electric vehicles, improvement in electric motor performance is directly linked to driving range and driving performance. In this paper, using an improved design for the interior permanent magnet synchronous motor (IPMSM), the EV driving range for the light-duty EV was extended. In the electromagnetic design process, a 2D finite element method (FEM) was used. Furthermore, to consider mechanical stress, ANSYS Workbench was adopted. To conduct a vehicle simulation, the vehicle was modeled to include an electric motor model, energy storage model, and regenerative braking. From these results, using the advanced vehicle simulator (ADVISOR) based on MATLAB Simulink, a vehicle simulation was performed, and the effects of the improved design were described.

Key Words : Electric Vehicle (EV), Saliency Ratio, Interior Permanent Magnet Synchronous Motor (IPMSM), Light-Duty Vehicle, Mechanical Stress, Power Density, Range Extension.

1. Introduction

These days, environmental problems from vehicle emissions such as carbon dioxide (CO2) and nitrogen oxide (NOx) are worsening. Because of an increasing number of cars and frequency of use, governments began to regulate vehicle emissions. For example, the European Union (EU) and the United States (US) suggested and enforced emission regulations. The EU initiated Euro 6 and is now applying Euro 6b. Euro 6c will be applied in 2020. The US federal Environmental Protection Agency (EPA) is now applying Tier II, and Tier III will be applied in 2017. Furthermore, to meet these trends, several nations offered electric vehicle and hybrid electric vehicle subsidies. For this reason, automotive makers started to develop environmentally friendly cars such as EVs, HEVs, PHEVs and FCEVs [1] - [3].

In particular, the light-duty vehicle as a city car and for personal mobility can easily implement EV characteristics because of its short driving range and restricted operating area. Moreover, its effects on emissions reduction would be significant because of high vehicle density resulting from heavy populations in cities. In addition, since the urban driving cycle involves much accelerating and decelerating, regenerative braking can save energy. We can also reduce noise pollution because of the EV's silent operation [4].

For xEV construction, such as battery based, or hybridized EV, the electric motor and the energy storage are the main components. Moreover, the electric motor is the most important part, since it acts like the internal combustion engine of a conventional vehicle. Thus, a significant amount of research into electric motors for xEV applications has been conducted across a wide range. This includes the control strategy, new topology, and improvements in efficiency. In particular, in light-duty EVs, the performance of the electric motor is directly linked to the driving performance of the EV. Moreover, improving the power density of the electric motor would appear to increase the overall efficiency of the vehicle because the weight of the electric motor weight is more important than that of conventional vehicles [5] - [7].

In this paper, a light-duty EV development scenario is introduced, extending the driving range, focusing on the electric motor design. Firstly, the IPMSM design process for EV application is demonstrated, improving power density and

* Corresponding Author : Dept. of Automotive Engineering, Hanyang University, Korea.
E-mail:hongjp@hanyang.ac.kr
* Dept. of Automotive Engineering, Hanyang University, Korea.
Received : October 19, 2016; Accepted : November 28, 2016

operating efficiency. Simultaneously, the mechanical stress and the maximum stress reduction are examined because of the high-speed operating conditions. After that, using an electric motor model, vehicle simulations are conducted with regard to the performance and efficiency of the electric motor. Consequently, the driving ranges of the IPMSM equipped EV are compared, between with the conventional and the improved electric motor model.

2. Improved Design

In this chapter, an improved design of the electric motor is created. First, a conventional model (to provide targets for the improved design) is introduced. It has an 8-pole/ 48-slot combination. Moreover, a process is described to improve the efficiency of the main operating region and the power density of the electric motor. Then mechanical stress was reduced by considering the centrifugal force of the rotor of the electric motor at its maximum speed. All the simulation results are finite element analysis (FEA) results.

2.1 Conventional Model

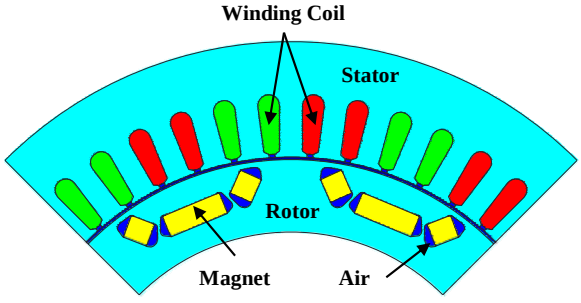

Fig. 1 Shape of the conventional model

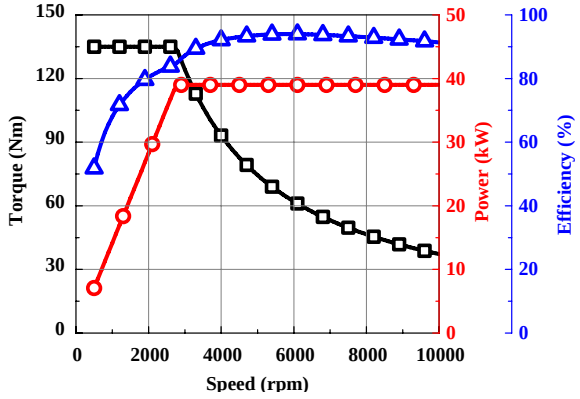

Fig. 2 Maximum performance curve of the conventional model

Table 1 Specification of the conventional model

Items	Value	Unit	Note
Pole / Slot Number	8 / 48	-	Distribution Winding
DC Link Voltage	380	V_{DC}	-
Maximum Speed	10000	rpm	-
Base Speed	2600	rpm	-
Maximum Torque	135	Nm	@ Base Speed
Maximum Power	39	kW	-
Stator Outer Diameter	280	mm	-
Rotor Outer Diameter	190	mm	-
Stack Length	42	mm	-

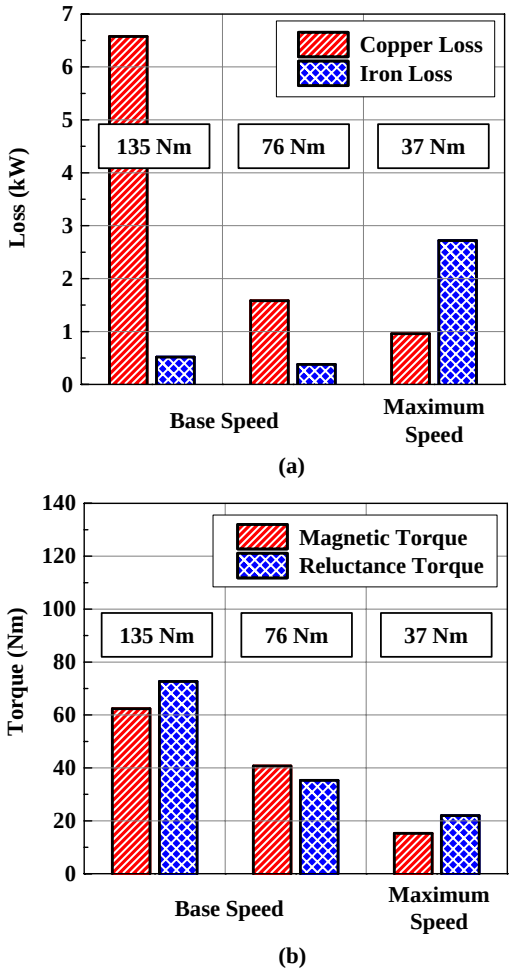

Fig. 3 Analysis result of the conventional model ((a) loss and (b) torque)

The conventional model of the electric motor, depicted in Fig. 1, is an 8-pole/48-slot interior permanent magnet synchronous motor (IPMSM) with a U-type inserted magnet. This model has a distribution winding with a five-coil pitch. Fig. 2 shows the maximum performance curve when the maximum torque per ampere (MTPA) control strategy

was applied [8].

The maximum power is 39 kW with a maximum torque and base speed, which is 143 Nm and 2600 rpm, respectively. The detailed specifications are listed in Table 1. Moreover, it has a high speed (10,000 rpm) condition, so we have to consider the iron loss, which is proportional to the operating speed. Fig. 3 describes these conditions, where (a) is the loss analysis result and (b) is the ratio between the magnetic torque and the reluctance torque from the 2D FEA at the rated power and maximum speed situation.

From the analysis results of the conventional model, copper loss in a high-torque operating condition and iron loss in a high-speed operating condition should be reduced. Moreover, if we raise the saliency ratio, defined as a difference between d-axis inductance and q-axis inductance, we could increase the reluctance torque. This design allows us to increase the torque per current, improving power density (torque density) while simultaneously reducing copper loss and iron loss.

2.2 Electromagnetic Design

There exist several losses in an electric motor: mechanical loss, iron loss, and copper loss. The mechanical losses come mainly from windage losses and bearing losses. The iron loss is generated at the magnetic core, when subjected to changing magnetic fields. There are hysteresis losses, eddy current losses, and anomalous losses. The copper losses result from current flowing in the copper winding. In fact, the eddy current loss of the inserted permanent magnet would be considerable, because of the high-speed operating condition. Also, this can be obtained easily from the 3-D FEA. However, that is not included in the scope of this paper, suggesting direction of the electric motor design for EV. Therefore, in this paper, the eddy current loss of the inserted permanent magnet is not considered. In this section we will discuss reducing iron loss and the copper loss, which can be achieved by redesigning the magnetic circuit[9].

First, a reduction in iron loss was achieved. Iron losses can be expressed as (1), following Steinmetz's equation, where B is the peak value of the magnetic flux density, α and β are the Steinmetz coefficients, and f is the frequency. The coefficients k_h, k_e, and k_a are coefficients of the hysteresis, eddy current, and anomalous losses, respectively. They are properties of the material [10].

$$W_{iron} = k_h f B^{\alpha} + k_e f^2 B^2 + k_a f^{1.5} B^{\beta} \quad (1)$$

To reduce the iron loss, the peak value of the magnetic flux density and frequency can be decreased. However, in automotive applications, high power density and high speed are mandatory conditions. In this paper, therefore, the core material was changed to have lower iron losses, as depicted in Fig. 4(a). The characteristics are listed in Table 2. This newly adopted electrical steel sheet has 53.3 % lower iron loss per kg at 100 Hz when the value of the magnetic flux density is 2.0 T. Fig. 4(b) shows the effects of the change in core materials on iron loss reduction [11].

Moreover, copper loss reduction was achieved in several ways. From the well-known equation of the electric motor output torque shown in (2), we can infer which parameter increases the output torque. P_n is the pole pair number, Ψ_a is the armature linkage flux, I_a is the armature current, β

Table 2 Properties of the core material

Items	50PN470	30PNF1600	Unit	Note
Thickness	0.5	0.3	mm	-
Density	7700	7600	kg/m^3	-
Maximum Iron Loss	4.70	2.16	W/kg	@ 50Hz, 1.5T
Tensile Strength	415	535	Mpa	Rolling direction
Yield Strength	275	410	Mpa	Rolling direction
Young`s Modulus	180	175	Gpa	-
Poisson`s Ratio	0.3	0.3	-	-

Table 3 Magnetic properties of the permanent magnet (Nd-Fe-B)

Items	N39UH	N42UH	Unit	Note
Residual Induction	1.15	1.27	T	@ 100℃
Intrinsic Coercive Force	1132	1190	kA/m	@ 100℃
Maximum Energy Product	286	318	kJ/m^3	@ 100℃
Recoil Permeability	1.05		-	-

is the armature current phase angle, L_q is the q-axis inductance, and L_d is the d-axis inductance. This equation can be separated for magnetic torque T_m owing to the rotor permanent magnet (3) and reluctance torque T_r from the rotor saliency (4) [12].

$$T = P_n \Psi_a I_a \cos\beta + \frac{1}{2}(L_q - L_d) I_a^2 \sin 2\beta \tag{2}$$

$$T_m = P_n \Psi_a I_a \cos\beta \tag{3}$$

$$T_r = \frac{1}{2} P_n (L_q - L_d)^2 I_a^2 \sin 2\beta \tag{4}$$

In the case of a fixed size in the radial direction, there are some ways to improve the torque density (power density) while simultaneously improving the efficiency. According to (2) – (4), given the conditions of maintaining the stator of the electric motor, enhancing the grade of the permanent magnet, and increasing the difference between the q-axis inductance L_q and the d-axis inductance L_d, the maximum torque per current can be increased. The former, enhancing the grade of the permanent magnet, increase the magnetic torque T_m from the relationship between the residual induction B_r of the permanent magnet and the amount of the linkage flux as described in (5), where W_m is the permanent magnet width and L_{stk} is the stack length of the rotor. And the latter, increasing the difference between the q-axis inductance and the d-axis inductance, secure the more reluctance torque T_r, following (4) [13],[14].

$$\Psi_a \propto B_r \times W_m \times L_{stk} \tag{5}$$

Fig. 5(a) shows a comparison of the magnetic properties according to the permanent magnet grades of N39UH and N42UH. N42UH has a high residual induction relative to N39UH, produces a large amount of linkage flux, and

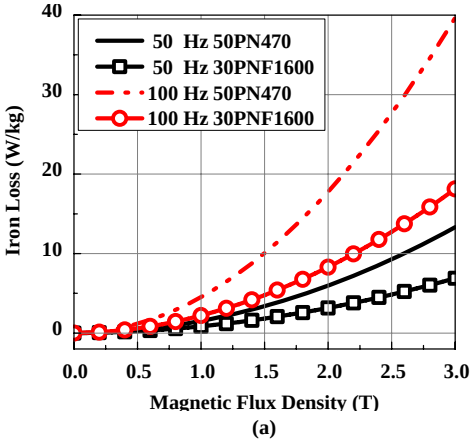

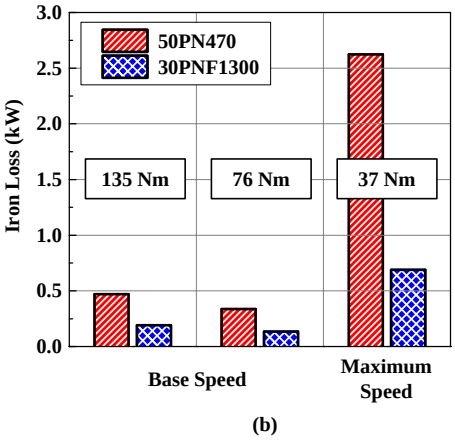

Fig. 4 Comparison between the conventional and the proposed core material ((a) iron loss and (b) its effect)

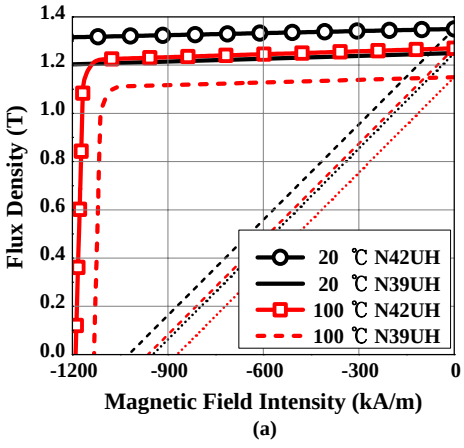

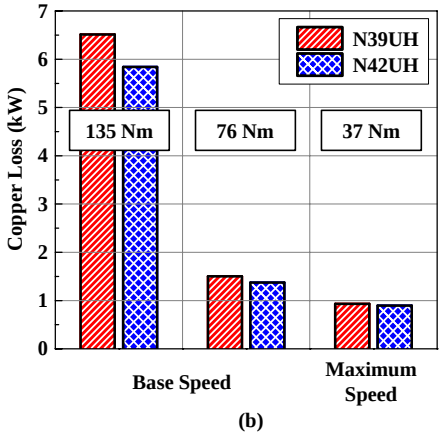

Fig. 5 Comparison between the permanent magnet grade ((a) the magnetic properties and (b) its effect)

generates more magnetic torque than N39UH. The characteristic values (such as the residual induction and coercive force) are shown in Table 3. The differences between the q-axis inductance and d-axis inductance according to the number of magnet layers are compared in Fig. 7. Fig. 5(b) shows the effect of permanent magnet grade on copper loss reduction.

Similar to the reluctance torque, the number of inserted magnet layers was a concern. If the number of magnet layers increased, the q-axis inductance would increase, resulting in increase of the difference between the q-axis inductance and d-axis inductance. However, Fig. 6 and Fig. 7 show the limits of the increase in difference between the q-axis and d-axis inductance resulting from the magnetic saturation effect on the q-axis magnetic flux path. An FEA simulation was performed using the maximum current conditions. From these results, the candidates for the number of magnet layers are two and three.

2.3 Mechanical Design

In the mechanical design of the electric motor, there are several issues with regard to mechanical stress, heat radiation, and assembly structure. For high-speed applications, mechanical stress in the rotor owing to centrifugal force should be considered. In this chapter, the mechanical stress was analyzed, and a design for mechanical stress reduction was performed.

First, the number of inserted permanent magnet layers was determined. From the results of Section 2.2, the candidates for the number of magnet layers were two and three. Using these models, a mechanical stress simulation was conducted by ANSYS with a von Mises equivalent stress. Fig. 8 shows the mechanical stress simulation results and the maximum stress at a maximum rotation speed of 10,000 rpm for each number of magnet layers. The maximum stress significantly increased when the number of

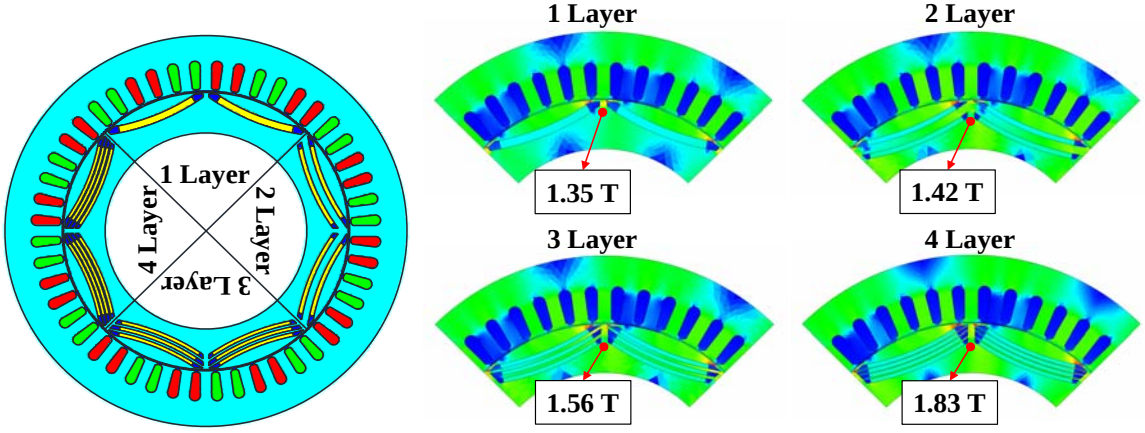

Fig. 6 Variation of the q-axis magnetic flux path flux density according to the number of the magnet layer

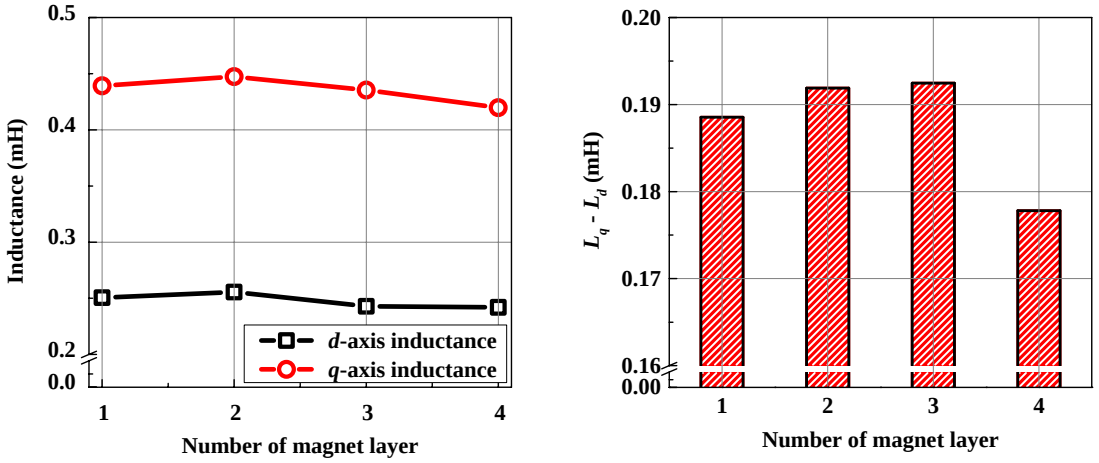

Fig. 7 Difference between q-axis inductance and d-axis inductance according to the number of the magnet layer

magnet layers was three. Consequently, the number of magnet layers was determined to be two.

Next, to increase the safety factor, a segment of an inserted magnet was conducted, thus reducing the maximum mechanical stress. As inserted magnet was segmented, the number of bridges increased. Mechanical stress is distributed to these bridges. The effect of the inserted magnet segment on mechanical stress reduction is shown in Fig. 9. However, segmenting the inserted magnet decreases the electrical performance because the leakage flux increases and the

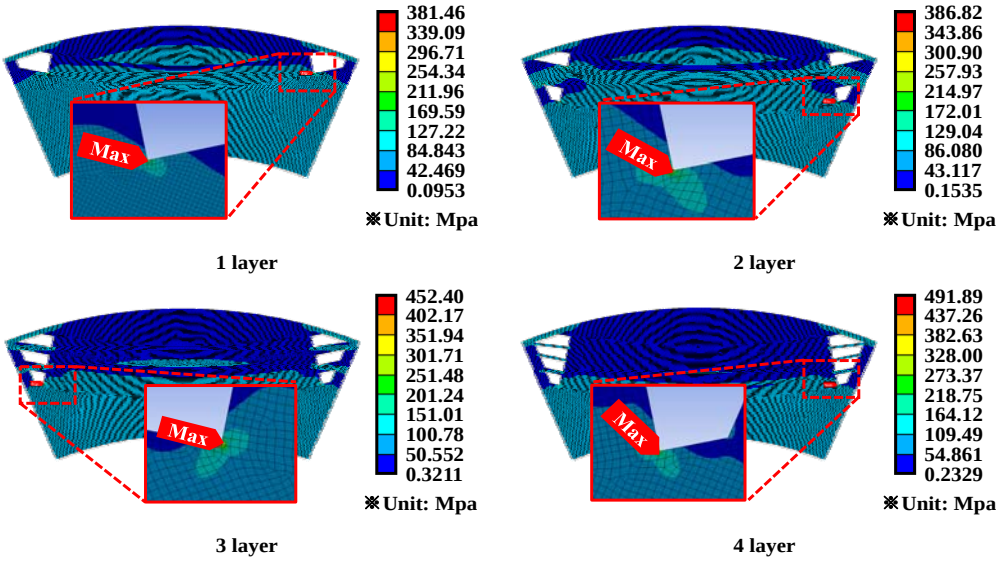

Fig. 8 The result of the mechanical stress simulation considering maximum rotating speed

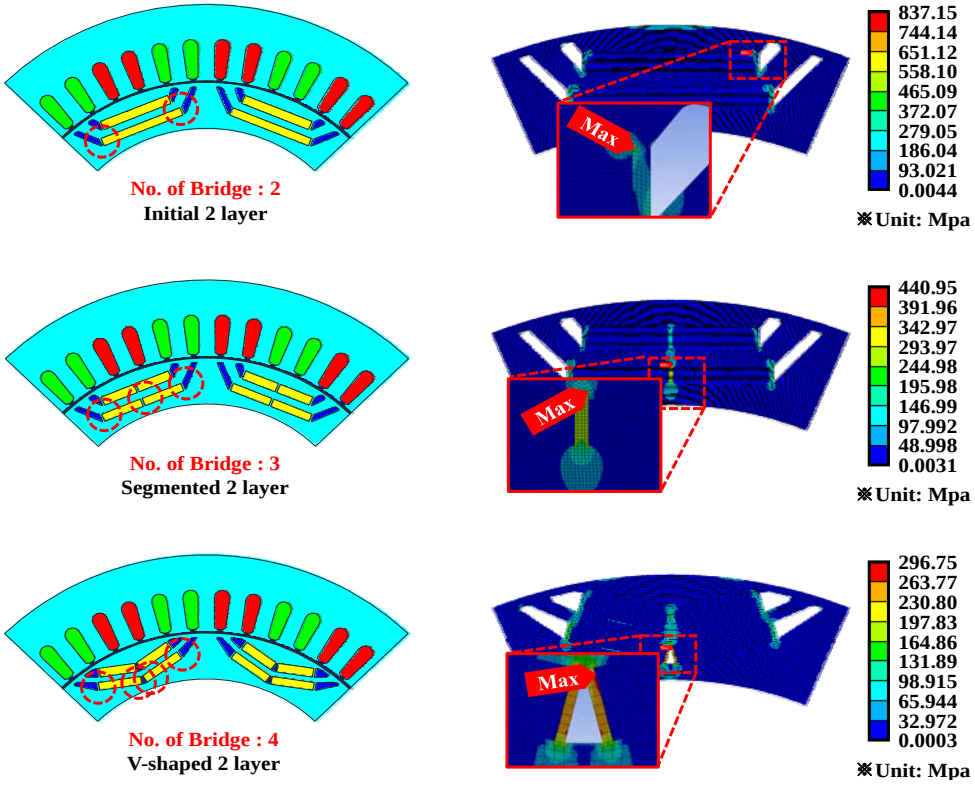

Fig. 9 The shape and the mechanical stress comparison between the initial 2-layer model and the segmented model

amount of the magnet decreases. For this reason, to supplement the insufficient amount of the magnet, a V-shaped magnet was adopted. Moreover, regarding the results, the number of the bridges increased. Fig. 9 also depicts the inserted V-shaped magnet and the results of the mechanical stress simulation.

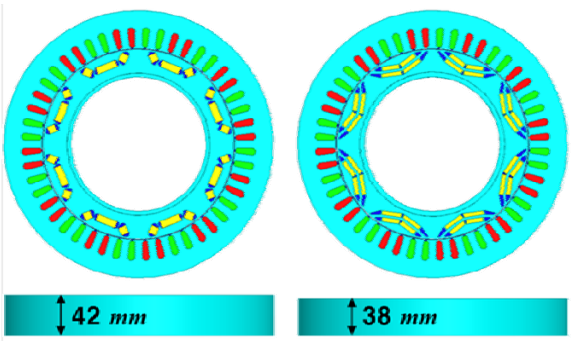

Fig. 10 Shape of the conventional model and the improved model

2.4 Design Result

Fig. 10 shows the shapes of the conventional model and the improved model. The stack length of the improved model decreased from 42 mm to 38 mm while maintaining

Table 4 Comparison of the conventional model and improved model

Items	Conventional	Improved	Unit
Stack Length	42	38	mm
Maximum Torque	135		Nm
DC Link Voltage	380		V_{DC}
Maximum Power	39		kW
Weight (Motor only)	12.5	11.0	kg
Weight(Include approximated weight of other part)	18.8	16.5	kg
Power Density (Include other part)	2.07	2.36	kW/kg
Maximum Mechanical Stress (Rotor)	263.95	296.75	Mpa
Yield Strength	275	410	Mpa
Safety Factor	1.04	1.38	-

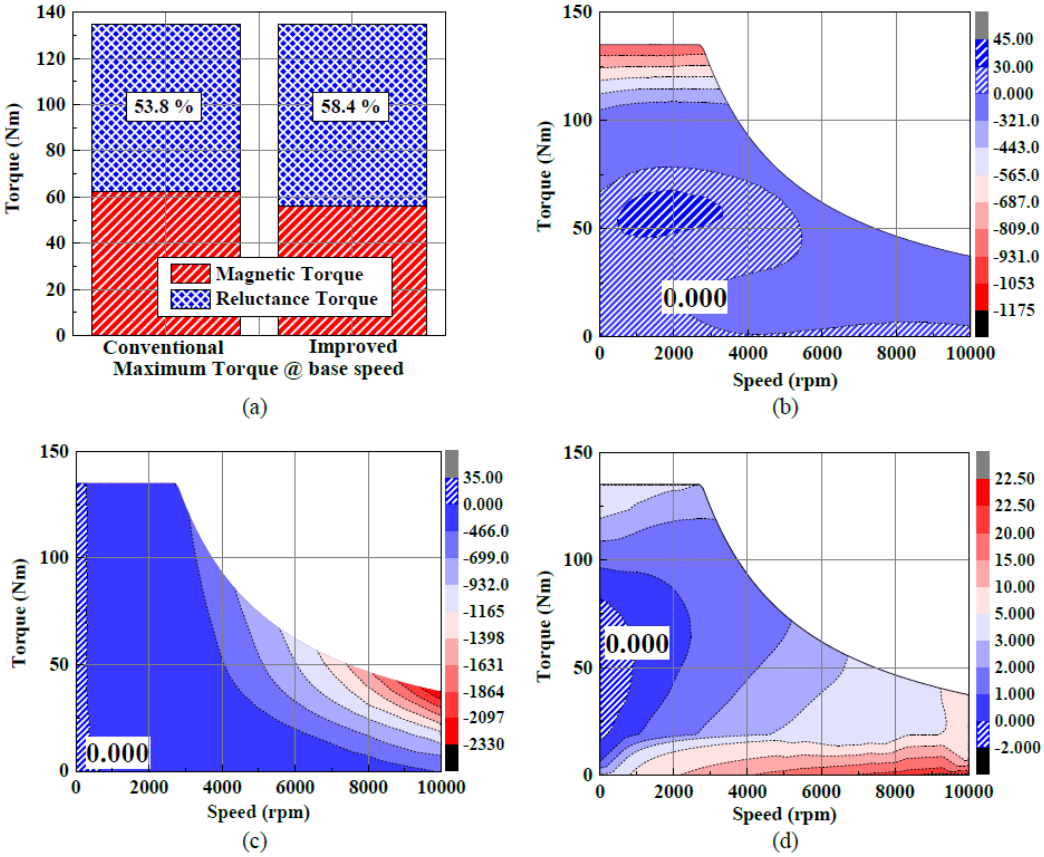

Fig. 11 Difference between the conventional model and the improved model (a) magnetic and reluctance torque,(b) copper loss, (c) iron loss, (d) efficiency

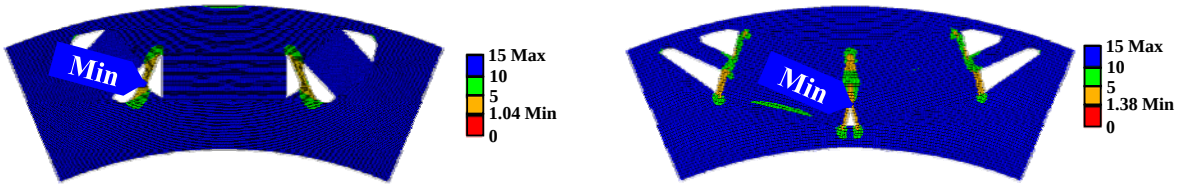

(a) (b)

Fig. 12 Comparison of the safety factor between the (a) conventional model and the (b) improved model

maximum output power. As a result, power density increased. Fig. 11(a) shows the increase in the ratio of the magnetic torque to the reluctance torque (53.8 % to 58.7 %) at the maximum torque base speed. Fig. 11(b) and (c) depict the changes in copper loss and iron loss. The hatched region indicates the increment of the losses, and the other region represents the decrease in the losses. Fig. 11(d) shows the improvements in efficiency, except for the hatched region of the contour. Moreover, the safety factor (the yield strength divided by the maximum stress) increased, as shown in Fig. 12.

3. Vehicle Modeling

In this chapter, to validate the effect of the improvement design, a vehicle model of the vehicle simulation is introduced. The specifications for the target EV, electric motor model, energy storage model, and consideration of regenerative braking were defined.

3.1 Target Vehicle

The target vehicle is the light-duty EV. This can be applied to a city car and for personal mobility. In this paper, a small light-duty EV for two people was adopted. Fig. 13 shows a schematic diagram of the EV used in the simulation. The energy storage supplies energy to the electric motor, and the electric motor's power is delivered to the drive line through a reduction gear. Moreover, regenerative braking occurs from the electric motor when the driver depresses the brakes. Detailed specifications including size and coefficient are listed in Table 5.

3.2 Electric Motor

An electric motor model was developed to reflect the characteristics of the electric motor design. From Chapter 2, a 2D FEM model was created for each model. One is a conventional model, and the other is an improved model.

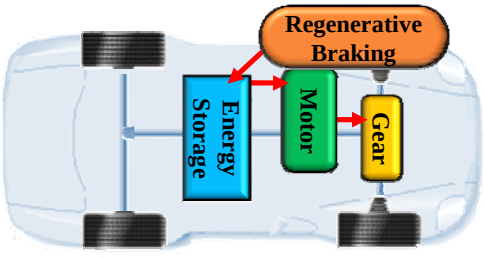

Fig. 13 EV schematic diagram

Table 5 Specification of the target vehicle

Items	Value	Unit	Note
Length	2345	mm	-
Width	870	mm	-
Height	1455	mm	-
Wheel Base	1695	mm	-
Wheel Radius	195	mm	-
Wheel Inertia	0.675	kgm^2	-
Gross Weight	240	kg	Except motor, battery weight
Rolling Resistance Coefficient	0.0086	-	-
Air Drag Coefficient	0.285	-	-

Through a 2D FEA, the linkage flux, d-q axis inductances, and iron losses were obtained for each operating condition.

Moreover, the phase resistance was calculated from the geometry information, and the copper losses were calculated simultaneously. Next, using the d-q axis equivalent circuit, efficiency was calculated for the torque-speed condition. Then efficiency maps were generated for the conventional model and the improved model. Fig. 14 describes the overall process of developing the electric motor model.

3.3 Energy Storage

The lithium-ion (Li-ion) battery was adopted for the EV. Similarly, an equivalent circuit model of the Li-ion battery was developed. This model consists of an open-circuit

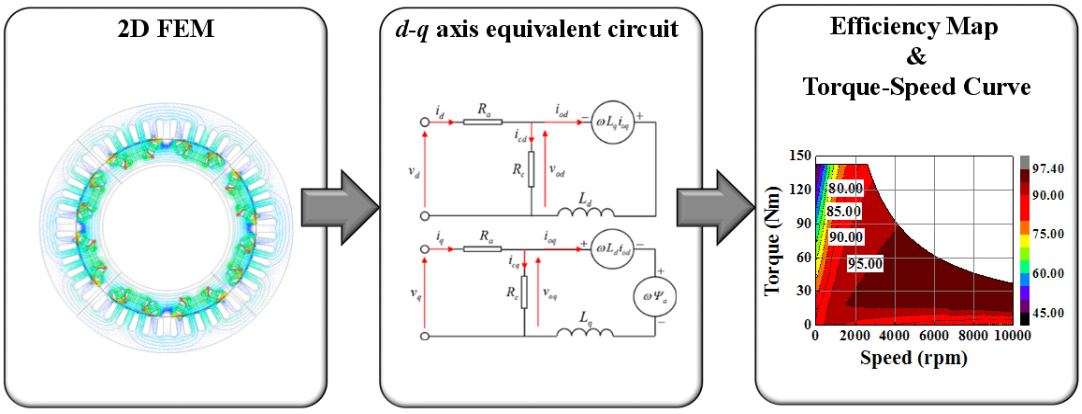

Fig. 14 Motor model generation

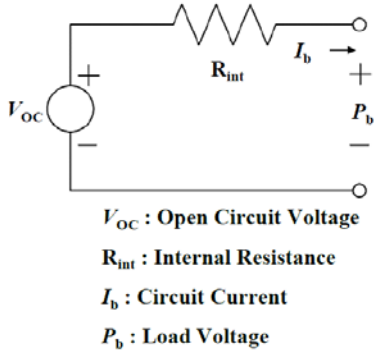

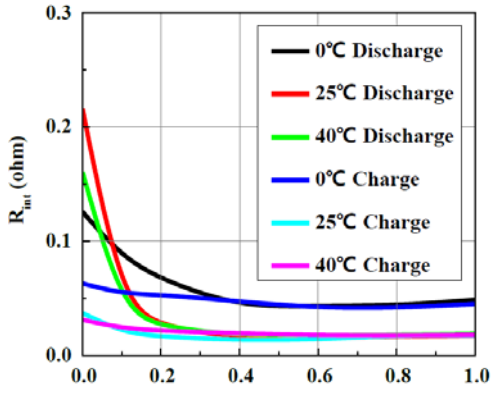

Fig. 15 Li-ion battery internal resistance (Rint) equivalent model

voltage V_{OC} and an internal resistance R_{int}. They are functions of the state of charge (SOC) and the temperature. The information for the parameters comes from the ADVISOR simulator developed by NREL. Fig. 15 shows the equivalent circuit model for R_{int}, and the R_{int} value according to the SOC and the temperature. Table 6 describes the Li-ion battery [15].

Table 6 Information of the Li-ion battery

Items	Value	Unit
Capacity	9.6	kWh
Nominal Voltage	534	V
Weight	47	kg
Power Density	204.25	Wh/kg

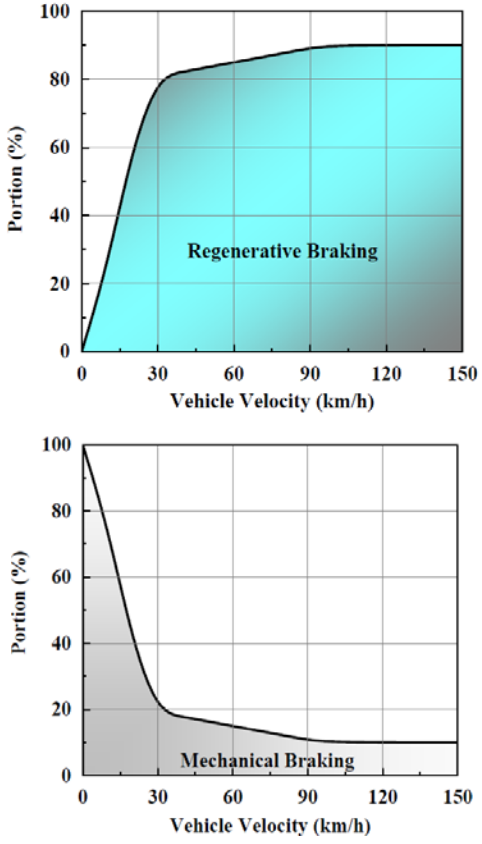

Fig. 16 Regenerative braking portion

3.4 Regenerative Braking

For xEV applications, regenerative braking is compulsory with regard to energy conservation. This can reduce mechanical braking losses and regenerate the energy that recharges the stored energy. Generally, the portion of regenerative braking is restricted because of safety and reliability. In this paper, the portion of regenerative braking was determined as described in Fig. 16.

4. Vehicle Simulation

Using the simulation models from Chapter 3, a vehicle simulation was performed. The Advanced Vehicle Simulator (ADVISOR) developed by National Renewable Energy Laboratory (NREL) of the U.S. department of energy (based on MATLAB Simulink) was adopted. Moreover, considering the driving cycle, the mileage and the energy consumption could be obtained.

4.1 ADVISOR

ADVISOR is an iterative vehicle simulation tool based on MATLAB Simulink. This program shows the results for energy consumption, grade ability, emissions, and other information for given conditions. Fig. 17 shows a block diagram of the EV simulation. During the simulation, the weight, air drag, and rolling resistance of the vehicle were considered. Moreover, the temperatures of the components were obtained from the loss look-up table and the heat capacity of each component, using the efficiency information. A motor model describing torque-speed curves and an efficiency map were applied to the electric motor part. A Rint model of the Li-ion battery was applied to the energy storage part, and regenerative braking was applied to the power bus part and control strategy part.

4.2 Driving Cycle

The driving cycle describes the vehicle velocity according to the time axis. Typically, the driving cycles reflect urban driving conditions and highway driving conditions. In this paper, three driving cycles were considered. The urban dynamometer driving schedule (UDDS) represents urban driving conditions, and US06HWY represents highway driving conditions. These were adopted and scaled to a maximum velocity of 60 km/h considering the target EV specifications.

Moreover, a driving cycle was created considering a UDO round-trip in the Jeju special self-governing province in Korea. In UDO, personal light-duty EVs are commercialized for tourists as round-trip vehicles. This driving cycle reflects the actual elevations along the driving path, which were obtained from GPS information. The scaled versions of UDDS and US06HWY are depicted in Fig. 18, and the UDO round-trip path description and its driving cycle are depicted in Fig. 19. A comparison of the driving cycles is listed in Table 7.

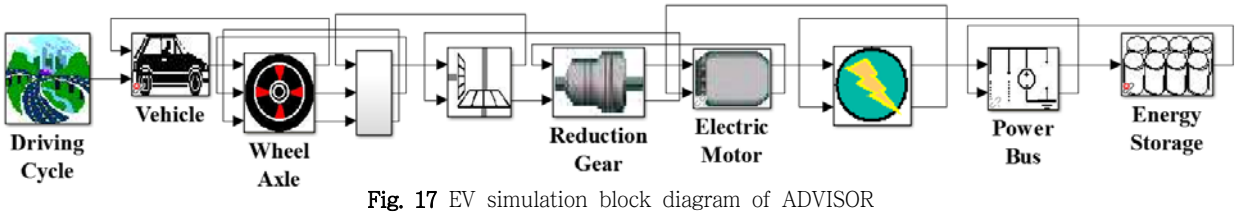

Fig. 17 EV simulation block diagram of ADVISOR

Table 7 Description of the driving cycle

Items	UDDS (Scaled)	US06HWY (Scaled)	UDO round-trip	Unit
Time	1369	368	1494	sec
Distance	7.88	4.66	14.53	km
Maximum Speed	60	60	60	km/h
Average Speed	20.72	45.46	35.01	km/h
Maximum Acceleration	0.97	1.43	1.64	m/s^2
Maximum Deceleration (-)	0.69	1.43	3.11	m/s^2
Idle Time	259	12	0	sec
Maximum Up Slope	-	-	15.5	%
Maximum Down Slope (-)	-	-	33.9	%

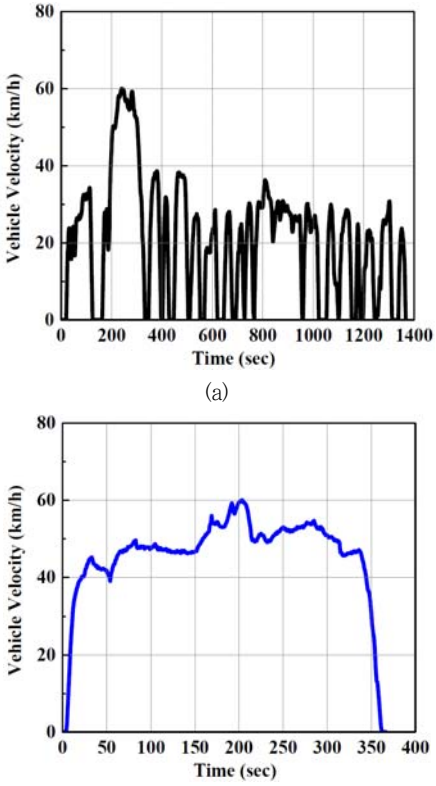

Fig. 18 Scaled driving cycle considering vehicle maximum velocity (a) UDDS (b) US06HWY

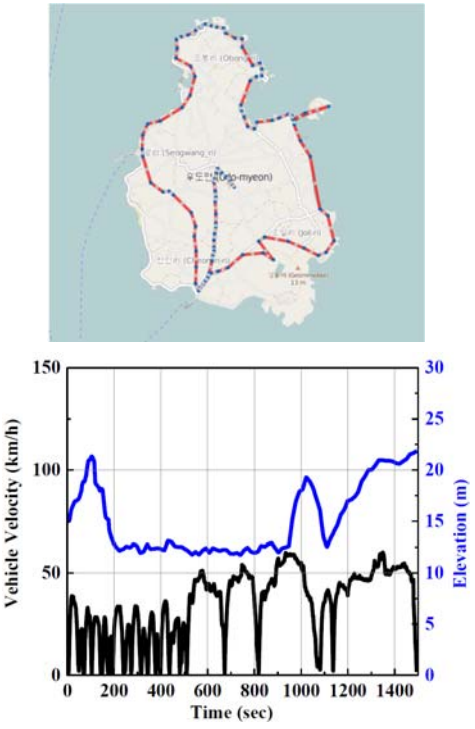

Fig. 19 UDO round-trip driving cycle considering elevation

5. Result

The simulation results for the electric motor operating point according to the driving cycle and differences in the efficiency map between the conventional model and the

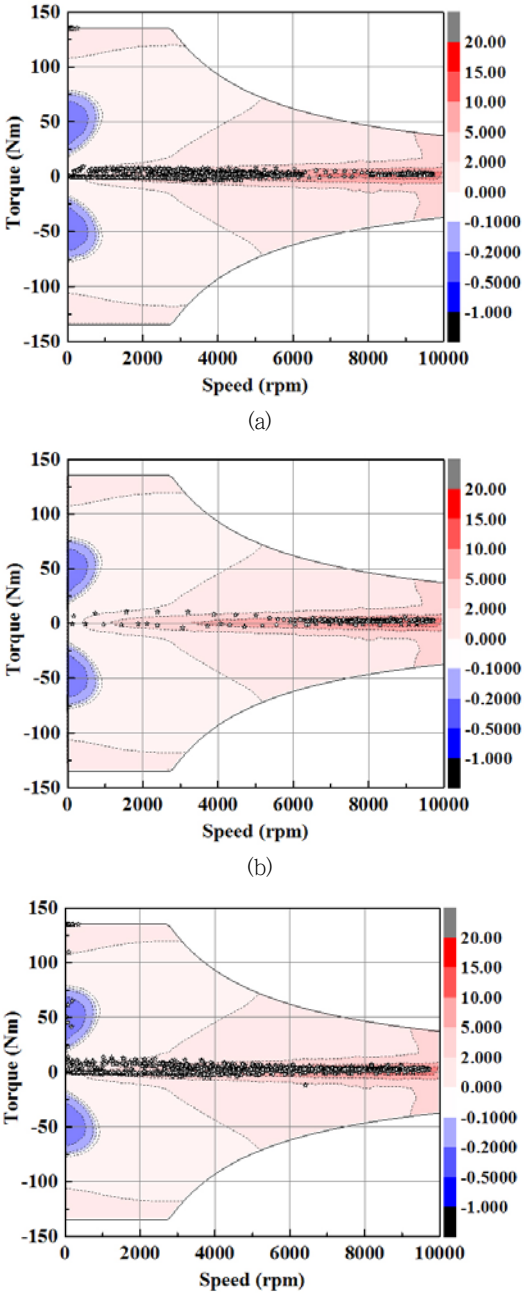

Fig. 20 Efficiency difference map of the (improved model - conventional model) and the operating point of the electric motor for given driving cycle (a) UDDS (Scaled)/ (b) US06HWY (Scaled)/ (c) UDO round-trip cycle

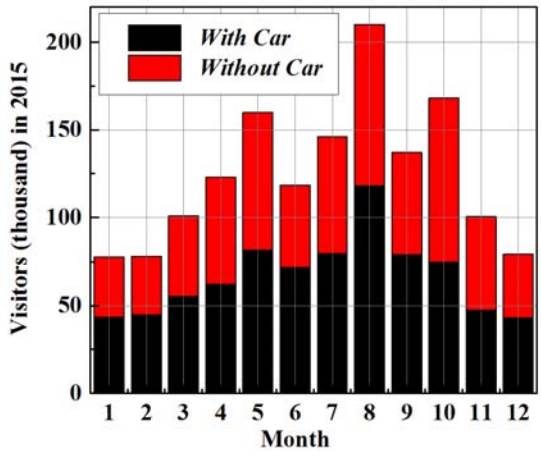

Fig. 21 UDO visitors in 2015

Table 8 UDDS (Scaled)

Items	Conventional	Improved	Unit
Overall Efficiency per Cycle	20.7	22.6	%
Remained SOC after one Cycle Operating	0.872	0.884	-
Maximum Driving Distance	58.9	64.5	km

Table 9 US06HWY (Scaled)

Items	Conventional	Improved	Unit
Overall Efficiency per Cycle	32.0	36.6	%
Remained SOC after one Cycle Operating	0.934	0.942	-
Maximum Driving Distance	67.1	76.7	km

Table 10 UDO Round-trip

Items	Conventional	Improved	Unit
Overall Efficiency per Cycle	26.8	30.1	%
Remained SOC after one Cycle Operating	0.776	0.801	-
Maximum Driving Distance	61.3	69.2	km

improved model are overlapped in Fig. 20. This shows that (b) US06HWY has the highest portion of the electric motor operating point in the highly improved efficiency region, and (a) UDDS has the lowest portion. Tables 8 to 10 describe this result. The increase in overall vehicle efficiency is as follows: (b) US06HWY 4.6 %, (c) UDO round-trip cycle 3.3 %, and (a) UDDS 1.9 %. Moreover, the extended ranges are (b) US06HWY 9.6 km, (c) UDO round-trip cycle 7.9 km, and (a) UDDS 5.6 km.

Table 11 Expectancy Effect of Improved Electric Motor on UDO Round-trip

Items (per year)	Conventional	Improved	Unit
Number of Overall Visitor Without Car	697604		-
Number of EV Rental Group	348802		-
Overall Distance	5068093.06		km
Distance per Full Charged EV	61.3	69.2	km
Number of Full Charged EV Battery for Overall Distance	82677	73238	-
Amount of Used Energy for Overall Distance	793.7	703.1	MWh

To examine the expected effects of this paper, an additional UDO round-trip simulation was conducted. Fig. 21 shows the visitors of the UDO in 2015. From this chart, the number of visitors without cars is 694,604. Assuming that pairs of visitors rented EVs, the resulting energy savings were analyzed. Table 11 shows the results. A total of 90.6 MWh per year was saved by using the EV battery.

6. Conclusion

An improved design for an electric motor was conducted. First, iron loss reduction was performed via an upgrade of the core material, resulting in highly reduced iron loss in the high-speed region. Second, copper loss reduction was achieved by raising the linkage flux and the reluctance torque. An increase in the flux linkage was accomplished by upgrading the permanent magnet. Securing the reluctance torque was achieved by increasing the difference between the q-axis inductance and the d-axis inductance. The number of inserted magnet layers was increased to two, also in order to increase the difference between the q-axis and d-axis inductances. Finally, because of the high-speed operating conditions, mechanical stress reduction was conducted.

To achieve the yield strength of the rotor and to consider safety factors, an inserted magnet was segmented. The insufficiency of the inserted magnet was reinforced by a V-shaped inserted magnet. Consequently, the improved model was designed with high efficiency and high power density and did not exceed the yield strength of the core material at the maximum rotation speed.

To validate the effect of the improved model on overall vehicle efficiency, vehicle modeling and simulation were performed. The target vehicle was a light-duty EV. The vehicle model consisted of vehicle specifications, the

efficiency and torque-speed curve of the electric motor, a Li-ion battery model, and a regenerative braking part. The vehicle simulation was conducted considering driving cycles. Three driving cycles were considered: scaled UDDS and US06HWY represent urban driving conditions and highway driving conditions, respectively, and the UDO round-trip cycle reflects the elevations of the driving path.

As a result, a range extension of the light-duty vehicle was achieved by improving the design of the electric motor in the range from the minimum 5.6 km to the maximum 9.6 km. From the results, a portion of the electric motor operating point is positioned in a region where efficiency has been highly improved, resulting in significant improvements in overall vehicle efficiency. Moreover, the UDO round-trip simulation result, which is the practical problem, shows that the 90.6 MWh energy can be saved per year.

Acknowledgement

"This research was supported by the MSIP(Ministry of Science, ICT and Future Planning), Korea, under the ITRC(Information Technology Research Center) support program supervised by the IITP(Institute for Information & communications Technology Promotion)"
(IITP-2016-H8601-16-1005)

References

[1] Worldwide Emissions Standards: Passenger Cars and Light Duty Vehicles, DELPHI, 2015.

[2] Gereon Meyer, Jadranka Dokic, Heike Jürgens, and Sebastian Stagle, "Hybrid and Electric Vehicles: The Electric Drive Delivers," Annual Report IEA IA-HEV Implementing Agreement for Co-operation on Hybrid and Electric Vehicle Technologies and Programmes, 2015.

[3] C. C. Chan, "The State of the Art of Electric, Hybrid, and Fuel Cell Vehicles," *IEEE Proc.*, vol. 95, pp. 704-718, 2007.

[4] Ennio Rossi, Carlo Villante, "A Hybrid City Car: Prototype by ENEA for Urban Mobility," *IEEE Vehicular Technology Magazine*, 2011.

[5] Di Pan, Kum-Kang Huh, and Thomas A. Lipo, "Efficiency Improvement and Evaluation of Floating Capacitor Open-Winding PM Motor Drive for EV Application," *IEEE Energy Conversion Congress and Exposition (ECCE)*, 2014.

[6] Myung-Seop Lim, Seung-Hee Chai, and Jung-Pyo Hong, "Design of Saliency Based Sensorless Controlled IPMSM with Concentrated Winding for EV traction," *IEEE Trans. Magn.*, vol. 52, No. 3, 8200504, March 2016.

[7] Sung-Jin Kim, Sang-Yong Jung, and Yong-Jae Kim, "Air-Barrier Width Prediction of Interior Permanent Magnet Motor for Electric Vehicle Considering Fatigue Failure by Centrifugal Force," *Journal of Electrical Engineering & Technology*, Vol. 10, pp. 952-957, 2015.

[8] Byeong-Hwa Lee, Soon-O Kwon, Tao Sun, Jung-Pyo Hong, Geun-Ho Lee, and Jin Hur, "Modeling of Core Loss Resistance for d-q equivalent Circuit Analysis of IPMSM considering Harmonic Linkage," *IEEE Trans. Magn.*, vol. 47, pp. 1066-1069, 2011.

[9] Jae-Woo Jung, Sang-Ho Lee, and Jung-Pyo Hong, "Optimum Design for Eddy Current Reduction in Permanent Magnet to Prevent Irreversible Demagnetization," Proceeding of International Conference on Electrical Machines and Systems, 2007.

[10] Rindra Ramarotafika, Abdelkader Benabou, Stéphane Clénet, and Jean Claude Mipo, "Experimental Characterization of the Iron Losses Variability in Stators of Electrical Machines," *IEEE Trans. Magn.*, vol. 48, pp. 1629-1632, 2012.

[11] Ji-Young Lee, Seung-Ryul Moon, Dae-Hyun Koo, Do-Hyun Kang, Geun-Ho Lee, and Jung-Pyo Hong, "Comparative Study of Stator Core Composition in Transverse Flux Rotary Machine," *Journal of Electrical Engineering & Technology*, vol. 6, pp. 350-355, 2011.

[12] Byeong-Hwa Lee, Jung-Pyo Hong, and Jung-Ho Lee, "Optimum Design Criteria for Maximum Torque and Efficiency of a Line-Start Permanent-Magnet Motor Using Response Surface Methodology and Finite Element Method," *IEEE Trans. Magn.*, vol. 48, pp. 863-866, 2012.

[13] Nobuyuki Matsui, Youji Takeda, Shigeo Morimoto, and Yukio Honda, Design and Control of IPMSM, Ohmsha, Ltd, 2001.

[14] Nicola Bianchi, Thomas M. Jahns, "Design, Analysis, and Control of Interior PM Synchronous Machine," *IEEE IAS Annual Meeting*, 2004.

[15] Jun-Hyeok Kim, Soon-Jeong Lee, Eung-Sang Kim, Seul-Ki Kim, Chul-Hwan Kim, and László Prikler, "Modeling of Battery for EV using EMTP/ATPD raw," *Journal of Electrical Engineering & Technology*, vol. 9, pp. 98-105, 2014.

저 자 소 개

김 동 민 (Dong-Min Kim)

Dong-Min Kim received Bachelor's degree in electronic information systems engineering from Hanyang University, Korea in 2013. Currently he is pursuing Ph.D. degree in automotive engineering from Hanyang University, Korea. His research interests are design and control of electric machine for automotive applications, and modeling of electric vehicles and hybrid electric vehicles.

정 영 훈 (Young-Hoon Jung)

Young-Hoon Jung received Bachelor's degree in mechanical engineering from Hanyang University, Korea in 2013. Currently he is pursuing Ph.D. degree in automotive engineering from Hanyang University, Korea. His research interests are electric machine design for automotive and industrial applications.

임 명 섭(Myung-Seop Lim)

Myung-Seop Lim received Bachelor's degree in mechanical engineering from Hanyang University, Korea in 2012. He received Master's degree in automotive engineering from Hanyang University, Korea in 2014. Currently he is pursuing Ph.D. degree in automotive engineering from Hanyang University, Korea. His research interests are electric machine design for automotive and robot applications, and sensorless drive.

심 재 한 (Jae-Han Sim)

Jae-Han Sim received the Bachelor's degree in mechanical engineering and the Master's degree in automotive engineering from Hanyang University, Seoul, Korea, in 2012 and 2014, respectively, where he is currently working toward the Ph.D. degree in automotive engineering. His research interests are the electric machines for automotive and industrial applications.

홍 정 표 (Jung-Pyo Hong)

Jung-Pyo Hong received the Ph.D. degree in electrical engineering from Hanyang University, Korea, in 1995. Since 2006 he has been working as a professor in the Hanyang University, Korea. His research interests are the design of electric machines, optimization and numerical analysis of electromechanics.